



V. Zega et alii, *Frattura ed Integrità Strutturale*, 29 (2014) 334-342; DOI: 10.3221/IGF-ESIS.29.29

Focussed on: Computational Mechanics and Mechanics of Materials in Italy

Integrated structure for a resonant micro-gyroscope and accelerometer

V. Zega, C. Comi, A. Corigliano

Department of Civil and Environmental Engineering, Politecnico di Milano, piazza Leonardo da Vinci 32, 20133 Milano, Italy.

valentina.zega@polimi.it, claudia.comi@polimi.it, alberto.corigliano@polimi.it

C. Valzasina

AMS Division, STMicroelectronics, via Tolomeo 1, 20010 Cornaredo, (Milano), Italy

carlo.valzasina@st.com

ABSTRACT. This paper presents the study of the mechanical behavior of a microstructure designed to detect acceleration and angular velocity simultaneously. The new resonant micro-sensor proposed, fabricated by the ThELMA[®] surface-micromachining technique, bases detection of two components of external acceleration (one in-plane component and one out-of plane component) and two components of angular velocity (roll and yaw) on the variation of frequency of several elements set in resonance. The device, despite its small dimensions, provides a differential decoupled detection of four external quantities thanks to the presence of four slender beams resonating in bending and four torsional resonators.

KEYWORDS. MEMS; Gyroscope; Accelerometer; Resonators.

INTRODUCTION

Micro-Electro-Mechanical Systems (MEMS) or microsystems, are micro-sized devices (see e.g. [1, 2]) nowadays largely used in the consumer and automotive market. Their diffusion is exponentially increasing in the biomedical market; their use is also growing in structural engineering as efficient and low-cost devices for structural health monitoring. Typical examples of widely diffused MEMS are accelerometers, gyroscopes, pressure sensors. The fast evolution of MEMS technology is mainly driven by the attempt to reduce the total size of the microsystem, while keeping the power consumption low and the sensitivity high enough for the specific applications. To reduce the cost and the dimensions required to embed several sensors for detecting the various external quantities, there is a trend to integrate a number of detection structures within the same device. Several proposals consists in integrating in a single die several sensors with different proof masses, a review of multi-DOF inertial MEMS is presented in [3]. Some interesting proposals also exist of multi-axial inertial sensors with a single proof mass: in [4] a five-axis sensor (3-axis accelerometer and 2-axis gyroscope) with capacitive detection was fabricated using silicon bulk micromachining; in [5] a six-axis vortex sensor (3-axis accelerometer and 3-axis gyroscope) with piezo-resistive detection was proposed.

In this line of research, in the present work we study an integrated structure for a micro-gyroscope and accelerometer. The device is fabricated by the Thelma[®] surface-micromachining technique [6] that makes it possible to obtain planar suspended structures with relatively small thickness, anchored to the substrate through flexible parts (springs) and



consequently able to displace with respect to the underlying silicon substrate. The proposed four-axis sensor makes use of differential resonant detection for both in-plane and out-of plane acceleration components and roll and yaw velocity components.

Resonant detection, as compared to other measuring techniques, has the advantage of affording a direct frequency output, of a quasi-digital type, a high sensitivity and a wide dynamic range. While several resonant accelerometers have been proposed in the literature [7-10] there exist a few examples of micro-gyroscopes with resonant detection [11-12].

The proposed device makes simultaneous use of two different operating principles typical of resonant MEMS: the frequency shift due to the presence of axial stresses in slender resonating beams and the frequency shift due to variations of the so-called electrical stiffness in torsional resonators. In particular, external in-plane acceleration or yaw velocity make the proof masses translate and induce axial forces in bending resonators, while external out-of-plane acceleration or roll velocity make the proof masses tilt and change the electrical stiffness of torsional resonators.

The paper is organized as follows. The first section presents the device design, discusses the mechanical behavior of the resonating parts and provides an analytical estimate of the sensitivity. The second section focuses on the fabricated device and presents the results of numerical modal simulations. Experimental characterization of the integrated sensor is currently under development.

DEVICE DESIGN

Device structure

The proposed structure is schematically shown in Fig. 1. The device is constituted by two moving proof masses attached to the substrate by means of folded springs which allow their translation in the plane and their tilting around the axes $a-a$. Four bending resonators (labelled I, II, III and IV in Fig. 1) are located beside the masses and attached to them through the external springs and four torsional resonators (labelled 1, 2, 3 and 4 in Fig. 1) are directly attached to the masses.

The variation of the resonance frequency in the flexural resonators is induced by the presence, upon translation of the inertial mass, of axial stresses while in the torsional resonators it is induced by variations of the so-called “electrical stiffness” to which the resonator mass is subjected. The simultaneous use of these two different type of resonators allows realizing of a four-axis sensor with reduced dimensions.

By means of the flexural resonator elements, the integrated detection structure enables differential detection of an angular velocity acting about an out-of-plane direction, the yaw angular velocity Ω_z , and of a linear acceleration a_y along the y -axis. In addition, by means of the torsional resonator elements, the integrated detection structure enables differential detection of an angular velocity acting about the y -axis, the roll angular velocity Ω_y , and of a linear out-of-plane acceleration a_z .

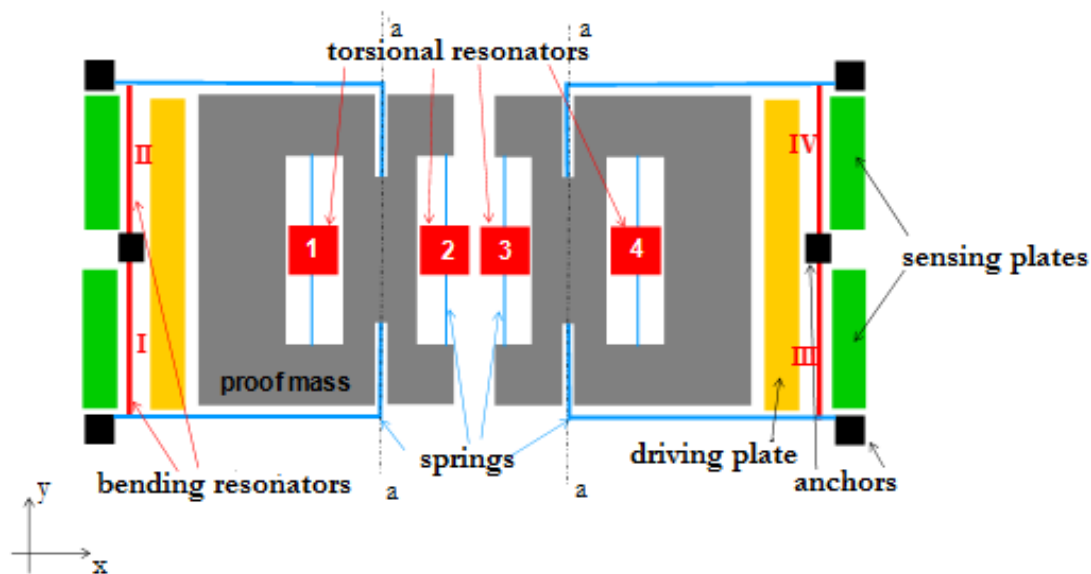


Figure 1: Schematic plan view of the structure, for detection of acceleration and angular velocity.

Bending and torsional resonators

We first focus on the modelling of the two types of resonator which constitute the sensing elements of the integrated structure.

The flexural resonators are very thin beams attached to the substrate at one end and to the springs at the other end, at a certain distance H from the anchor point (see Fig. 2(a)). The optimal length of H is selected to maximize the sensitivity of the device. The electrostatic driving of the resonator is done by means of an electrode attached to the substrate with initial gap d_0 ; another parallel electrode allows for the sensing. During functioning a polarization voltage V_p is applied to the resonator while a small oscillating signal $v_a(t)$ applied to the driving plate drives the beam to resonance.

In the absence of external input, the resonator has the nominal frequency f_0

$$f_0 = \frac{1}{2\pi} \sqrt{\frac{k_m - k_e}{m}} \tag{1}$$

where k_m , k_e and m are the equivalent mechanical and electrostatic stiffness and the equivalent mass, respectively.

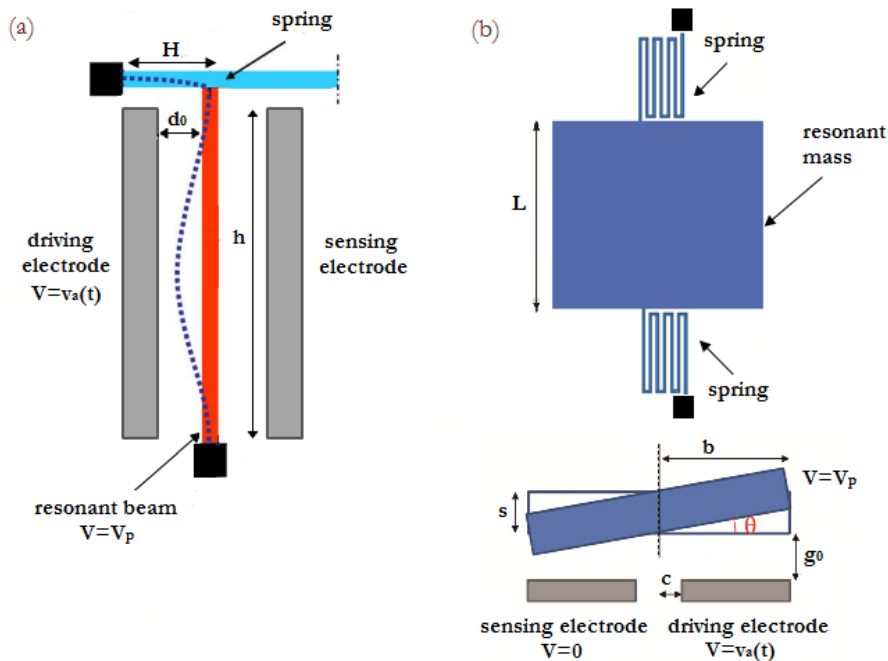


Figure 2: Schematic views of the resonators: (a) in-plane view of bending resonator, (b) in-plane and side view of torsional resonator

Their expressions can be obtained as in [13] making use of the Hamiltonian's principle and searching for the solution, in terms of transverse displacement of the beam, in the form $w(y,t) = \psi(y)W(t)$. Using as $\psi(y)$ the eigenfunction of a doubly clamped beam these equivalent properties read:

$$\begin{aligned} k_m &= \int_0^b EI(\psi''')^2 dy = 198.492 \frac{EI}{b^3} \\ k_e &= \int_0^b 2 \frac{\epsilon_0 s V_p^2}{d_0^3} \psi^2 dy = 2 \frac{\epsilon_0 s V_p^2}{d_0^3} 0.397b \\ m &= \int_0^b \rho A \psi^2 dy = 0.397 \rho A b \end{aligned} \tag{2}$$

where E is the Young's modulus, A and I the area and the momentum of inertia of the cross section, ϵ_0 is the dielectric permittivity, s is the out of plane thickness and ρ the mass density.



When, due to an external acceleration or yaw angular velocity, the in-plane inertia force or the Coriolis' force is applied to the proof masses, an axial force N is exerted on the resonators and their frequency changes according due to an additional geometric stiffness term k_G

$$k_G = \int_0^b N (\psi')^2 dy = \frac{4.88}{b} N \tag{3}$$

In the case of a tensile axial load N the beam oscillation frequency increases while in the case of a compressive load it decreases [14-16] according to the relation:

$$f = \frac{1}{2\pi} \sqrt{\frac{k_m + k_G - k_e}{m}} = f_0 \sqrt{1 + \frac{4.88}{b(k_m - k_e)} N} \tag{4}$$

Since the resonating beam is very slender and the gap d_0 is very small, nonlinear effects can appear due to both geometrical and electrostatic effects. However, the presence of the little horizontal part of length H , see Fig. 2(a), partially releases the axial constraint, thus lowering the higher order mechanical stiffness terms and widening the regime of linear oscillation. The electrostatic stiffness nonlinearities can be reduced by lowering the actuation voltage $v_d(t)$; the sensor proposed in this work will be actuated in the linear regime. A detailed discussion on the nonlinear behavior of the resonator can be found in [13,17].

The other resonators included in the device are torsional resonators constituted by a small mass of in-plane dimensions $2b \times L$ and out-of-plane thickness s connected to the proof mass by two folded torsional springs, which allow for its out-of-plane rotation $\theta(x,t)$ (see Fig. 2(b)). When in the rest position, the mass is at distance g_0 from both the electrodes (see Fig. 2(b)) and the torsional resonator has the nominal frequency φ_0

$$\varphi_0 = \frac{1}{2\pi} \sqrt{\frac{K_m - K_e}{\rho J_{mass}}} \tag{5}$$

with

$$K_m = \frac{2GJ}{l}, \quad K_e = \frac{2\epsilon_0 L}{3g_0^3} V_p^2 (b^3 - t^3)$$

where J is the torsional momentum of inertia, ρJ_{mass} is the centroidal mass moment of inertia of the rigid mass, l is the total length of one of the folded torsional springs and G is the shear elastic modulus.

The sensing electrode is usually connected to a virtual ground at zero voltage while the mass is kept at the polarization fixed voltage V_p (see Fig. 2(b)). By applying a small variable voltage $v_d(t)$ to the driving electrode the mass is electrostatically actuated and can dynamically vibrate.

When, due to external actions, the proof masses tilt, there is a change of gap g_0 between the resonators and the electrodes and the frequency changes according to equation (5).

As for the bending resonators nonlinear effects can appear for high values of $v_d(t)$ due to higher order terms in the electrostatic stiffness. The nonlinear behavior and the range of actuation available to ensure operation in the linear regime are studied in [18].

Device operation principle

During the gyroscope-accelerometer functioning the inertial proof masses are kept in resonance according to their in-plane translational mode in x direction by means of electrostatic driving implemented by the respective driving electrodes (see Fig. 1).

Also the bending resonator elements (labeled I, II, III, IV in Fig. 3) are kept in resonance according to the first flexural mode in the plane along the first axis x , by means of electrostatic interaction with the driving electrodes. In absence of an external angular velocity or linear acceleration, all resonators have the same nominal frequency f_0 , see eq. (1).

When an external yaw angular velocity Ω_z is applied, two Coriolis' forces F_c originate on the two inertial masses; they are directed along the axis y , have opposite signs (see Fig. 3(a)) and have modulus:

$$F_c = 2m\Omega_z \dot{x} \tag{6}$$

where \dot{x} is the linear velocity of the inertial masses due to resonant driving and m is their mass.

Consequently, the resonators, are subjected to an axial action: in particular, two of them, for instance resonators I and IV, are subjected to a compressive force, whereas the other two, for instance II and III, are subjected to a tensile force of the same intensity, N ,

$$N_{II} = N_{III} = -N_I = -N_{IV} = \gamma \frac{F_c}{2} \quad (7)$$

where γ is a force-amplification factor, depending on the geometry of the resonator and in particular on H .

Because of the axial stress, the frequency of oscillation of the resonators subjected to compression decreases, whereas the frequency of oscillation of the resonators subjected to tension increases, according to the relation (4).

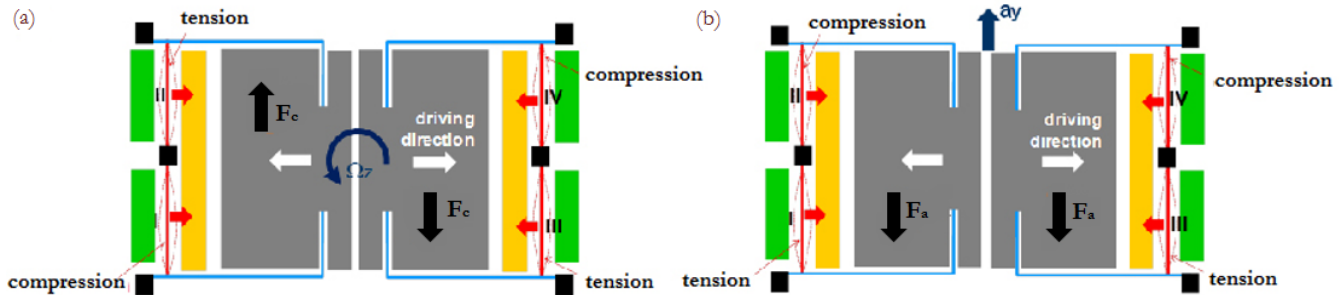


Figure 3: Schematic plan view of the structure: (a) detection of the yaw angular velocity Ω_z , (b) detection of the linear acceleration a_y

Combining the readings of frequency of the four bending resonators from equation (4), linearized around the nominal frequency f_0 , one can compute the external yaw angular velocity Ω_z

$$\begin{aligned} f_{III} + f_{II} - f_I - f_{IV} &\approx 2f_0 \left(1 + \frac{1}{2} \frac{4.88}{b(k_m - k_e)} \gamma m \Omega_z \dot{x} - 1 + \frac{1}{2} \frac{4.88}{b(k_m - k_e)} \gamma m \Omega_z \dot{x} \right) = \\ &= 2f_0 \frac{4.88}{b(k_m - k_e)} \gamma m \Omega_z \dot{x} \end{aligned} \quad (8)$$

On the other hand, when an external linear acceleration a_y is applied, as shown in Fig. 3(b), the inertial masses are subjected to inertia forces F_a directed in the y direction, with the same sign and with modulus

$$F_a = m a_y \quad (9)$$

As a result of the inertia forces F_a , the bending resonators are again subjected to axial stresses, but in this case, these axial stresses are of the same sign in the resonators I and III, and they are of the same sign in the resonators II and IV.

$$-N_{II} = N_{III} = N_I = -N_{IV} = \gamma \frac{F_a}{2} \quad (10)$$

Combining the readings of the four resonators starting once again from equation (4) linearized around the nominal flexural oscillation frequency f_0 , one obtains a measure of the external acceleration a_y :

$$f_I + f_{III} - f_{II} - f_{IV} \approx 2f_0 \left(1 + \frac{1}{4} \frac{4.88}{b(k_m - k_e)} \gamma m a_y - 1 + \frac{1}{4} \frac{4.88}{b(k_m - k_e)} \gamma m a_y \right) = f_0 \frac{4.88}{b(k_m - k_e)} \gamma m a_y \quad (11)$$

Therefore, via a different combination of the quantities supplied by the same resonator elements it is possible to detect simultaneously the yaw angular velocity Ω_z and the linear in-plane acceleration a_y ; both measures are of differential type.

The measure of the roll angular velocity Ω_y and of the linear out-of-plane acceleration a_x is performed by means of the torsional elements labeled 1, 2, 3, 4 in Fig. 4, kept in resonance according to their torsional natural mode through the driving electrode located below them on the substrate.

When an external roll angular velocity Ω_y is applied, two Coriolis' forces, labeled F_c in Fig. 4(a), originate on the inertial masses which are oscillating in the x -direction. These forces are directed along the out-of-plane axis z , have opposite signs and the modulus is given by

$$F_c = 2m\Omega_y \dot{x} \tag{12}$$

As a result, the two inertial masses rotate about their respective axis of rotation *a-a* in the same direction (see Fig. 4(a)) of the angle:

$$\beta = 3 \frac{m\Omega_y \dot{x} R_G}{G_s \bar{l}^3} \bar{l} \tag{13}$$

where R_G is the distance between the *a-a* axis of rotation of a proof mass and the center of gravity of the same mass, \bar{l} is the total length of one folded torsional spring attaching the mass to the substrate and \bar{l} its in-plane thickness.

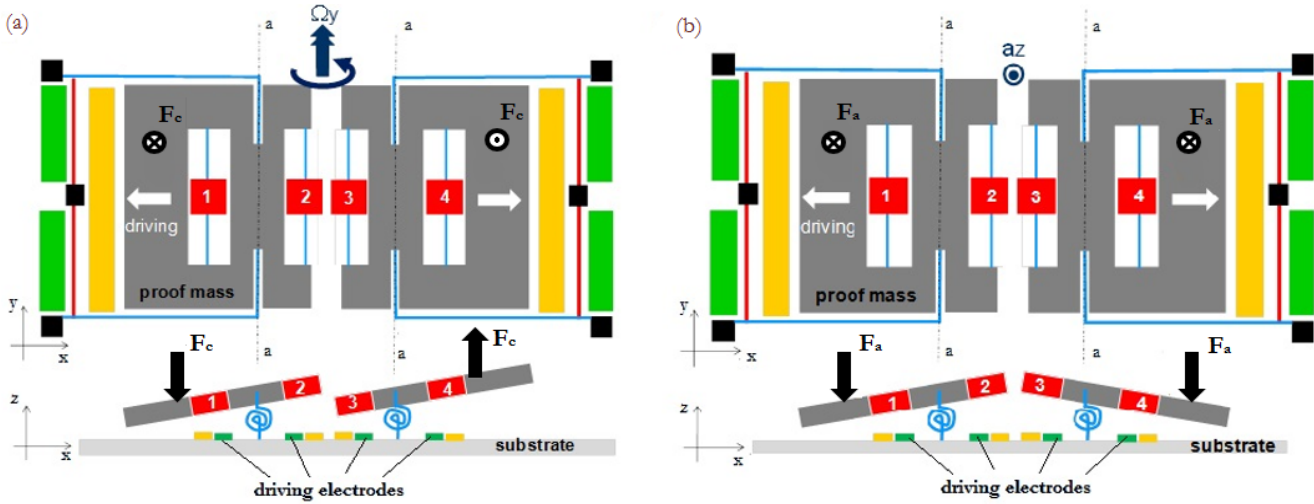


Figure 4: Schematic plan view of the structure: (a) detection of the roll angular velocity Ω_y , (b) detection of the linear acceleration a_z .

In particular, a first resonator element approach the substrate and its gap reduces to $g_0 - R\beta$ while the other resonator element move away from the same substrate and its gap increases to $g_0 + R\beta$, R being the distance between the *a-a* axis and the torsional resonator's axis of rotation. The torsional resonators change their natural frequencies according to (5) as a consequence of their electrostatic stiffness variation

$$\varphi_1 = \varphi_3 = \frac{1}{2\pi} \sqrt{\frac{K_m - \frac{2\varepsilon_0 L}{3(g - \beta R)^3} V_p^2 (b^3 - c^3)}{\rho J_{mass}}}, \quad \varphi_2 = \varphi_4 = \frac{1}{2\pi} \sqrt{\frac{K_m - \frac{2\varepsilon_0 L}{3(g + \beta R)^3} V_p^2 (b^3 - c^3)}{\rho J_{mass}}} \tag{14}$$

By combining the readings of the four torsional resonators and linearizing one obtains the frequency shift which provides a differential measure of the roll angular velocity Ω_y :

$$\varphi_2 - \varphi_1 + \varphi_4 - \varphi_3 \approx 6\varphi_0 \frac{K_e}{K_m - K_e} \frac{R}{g_0} \beta = 18\varphi_0 \frac{K_e}{K_m - K_e} \frac{R}{g_0} \frac{m \dot{x} R_G}{G_s \bar{l}^3} \bar{l} \Omega_y \tag{15}$$

In the presence of linear out-of-plane acceleration a_z (see Fig. 4(b)), two forces of inertia F_a originate on the two inertial masses directed along the axis z , which have in this case the same sign. Because of these forces, one inertial mass rotates counterclockwise, while the other rotates clockwise by an angle:

$$\beta = \frac{3}{2} \frac{m a_z R_G}{G_s \bar{l}^3} \bar{l} \tag{16}$$

In this case, therefore, frequency variations of the same sign occur in the torsional resonator elements 1 and 4, and in the torsional resonator elements 2 and 3. Similarly to what done for the measure of the roll velocity, combining the readings of the four torsional resonators, the following expression is obtained, allowing for the measure of the external acceleration a_z :

$$\varphi_2 - \varphi_1 + \varphi_3 - \varphi_4 \approx 6\varphi_0 \frac{K_e}{K_m - K_e} \frac{R}{g_0} \beta = 9\varphi_0 \frac{K_e}{K_m - K_e} \frac{R}{g_0} \frac{mR_G}{G_s T^3} \bar{l} a_\zeta \quad (17)$$

FABRICATED DEVICE

The designed integrated structure has been produced with the surface micromachining process ThELMA[®] which has been developed by STMicroelectronics to realize silicon inertial sensors and actuators.

The main process phases are substrate thermal oxidation, deposition and patterning of horizontal interconnections, deposition and patterning of a sacrificial layer, epitaxial growth of the structural layer, structural layer patterning by trench etch and sacrificial oxide removal and contact metallization deposition (see [6] for more details).

The inertial masses of the integrated structures and the proof masses of the torsional resonators have holes to allow the complete oxide removal below it.

The produced integrated structure is shown in the SEM micrograph of Fig. 5.

The integrated structure is packed at the pressure of 1mbar with getter to avoid degasing.

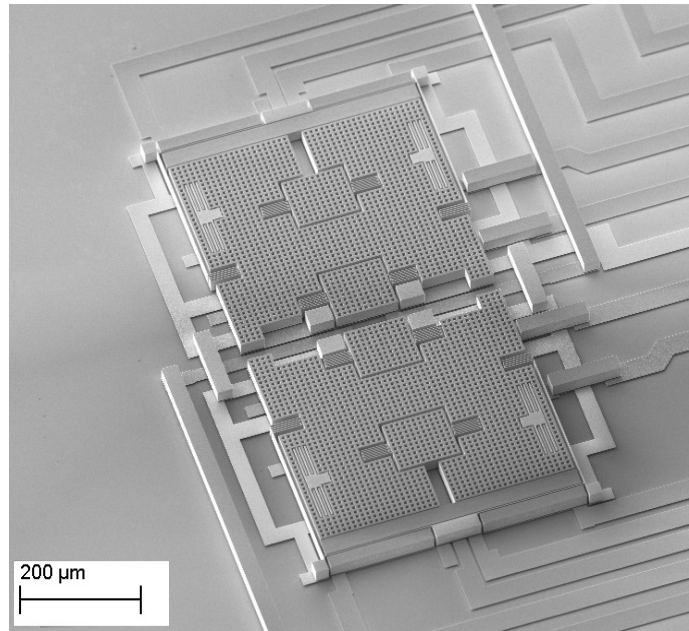


Figure 5: SEM image of the integrated structure for a resonant micro-gyroscope and accelerometer

Numerical analyses

The eigenmodes of the device have been calculated through a three dimensional finite element analysis performed by the commercial code COMSOLMultyphysics[®]: the first 6 modes together with the first bending mode of the beam resonators (21st mode for the whole structure) are reported in Tab. 1 along with small pictures of the corresponding modal shape. For the sake of an easier visualization, the contours of the magnitude of the displacement are shown on the modal shapes. The driving modes for the inertial masses is around 10 kHz, the natural frequency of the torsional resonators is 22.5 kHz and the natural frequency of the bending resonators is 243 kHz.

Note that the resonators have been designed to oscillate at very different frequencies in order to obtain similar sensitivities for the out-of-plane and in-plane external acceleration and angular velocity components. The separation of the frequencies also ensure a very low cross-talk in sensing.

With a size of the two inertial masses of approximately 420 μm x 470 μm x 22 μm and a bias voltage of 6V, the expected sensitivity as accelerometer in both of the directions y and z is higher than 350 Hz/g, while the sensitivity as gyroscope is approximately 0.15 Hz/°/s.

The experimental characterization of the device is currently under development.



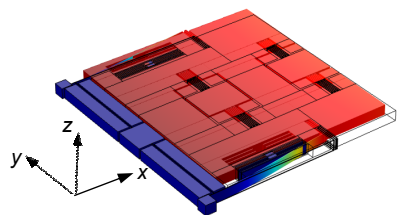
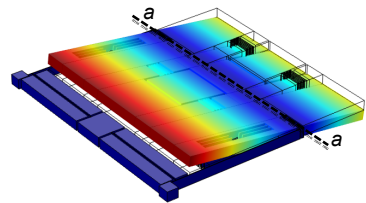
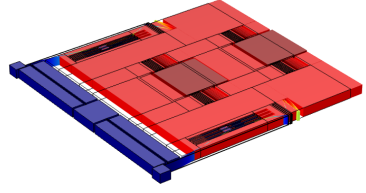
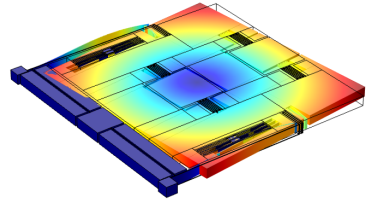
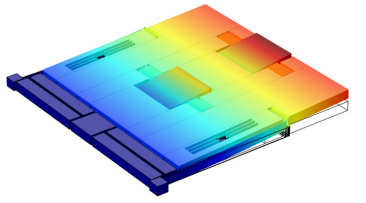
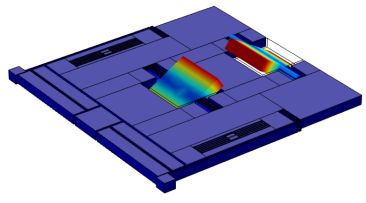
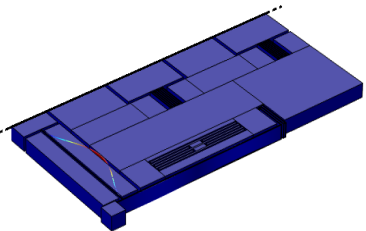
Mode #	Frequency (kHz)	Description	
1	1.33	In-plane translation of the whole mass along y-axis	
2	2.26	Out-of-plane rotation of the whole mass around axis $a-a$	
3	10.11	In-plane translation of the whole mass along x-axis (driving mode)	
4	12.61	In-plane rotation of the whole mass around z-axis	
5	13.44	Torsional mode of the proof mass	
6	22.52	First mode of torsional resonators	
21	243	First mode of bending resonators	

Table 1: Principal modes of the device. Because of the device's symmetry only one half of it is plotted.



CONCLUSION

In the present work, an innovative resonant four-axis inertial sensor has been designed, modelled and fabricated. Analytical and numerical finite elements simulations have been used during the design phase for the evaluation of the device performances and for the maximization of its sensitivity.

The resulting structure has only two inertial masses and, despite its extremely reduced dimensions, enables differential detection of two different angular velocities and of two different linear acceleration components. Resonant detection is used for the four axis, with two different kind of resonators respectively oscillating in bending and in torsion.

The differential reading enables detection of the external quantities even in the presence of eigenstresses due e.g. to temperature variations. Moreover, the differential reading increases the range of linearity and the sensitivity of the proposed inertial sensor.

REFERENCES

- [1] Senturia, S.D., *Microsystem design*, Kluwer Academy, Dordrecht (2002).
- [2] Gardner, J.W., Varadan, V.K., Awadelkarim, O.O., *Microsensors MEMS and smart devices*, Wiley, Chichester (2001).
- [3] Ayazi, F., Multi-DOF inertial MEMS: From gaming to dead reckoning, Proc. 16th International Solid-State Sensors, Actuators and Microsystems Conference, TRANSDUCERS'11, (2011) 2805-2808.
- [4] Watanabe, Y., Mitsui, T., Mineta, T., Kobayashi, S., Taniguchi, N., Okada, K., Five-axis motion sensor with electrostatic drive and capacitive detection fabricated by silicon bulk micromachining, *Sens. Actuator A*, 97-98 (2002) 109-115.
- [5] Xie, Z., Chang, H., Yang, Y., Li, X., Zhou, P., Yuan, W., Design and fabrication of a vortex inertial sensor consisting of 3-DOF gyroscope and 3-DOF accelerometer, In: Proc. of the IEEE International Conference on Micro Electro Mechanical Systems (MEMS), (2012) 551-554.
- [6] Corigliano, A., Masi, B.D., Frangi, A., Comi, C., Villa, A. and Marchi, M., Mechanical characterization of polysilicon through on chip tensile tests, *J. Microelectromech. Syst.*, 13 (2004) 200-219.
- [7] Zhu, R., Zhang, G., Chen, G., A novel resonant accelerometer based on nanoelectromechanical oscillator, In: Proc. MEMS 2010, Hong Kong, (2010) 440-443.
- [8] Comi, C., Corigliano, A., Langfelder, G., Longoni, A., Tocchio, A., Simoni, B., A resonant micro-accelerometer with high sensitivity operating in an oscillating circuit, *J. Microelectromech. Syst.*, 19 (2010) 1140 – 1152.
- [9] Kim, H.C., Seok, S., Kim, I., Choi, S-D. , Chun, K., Inertial-grade out-of-plane and in-plane differential resonant silicon accelerometers (DRXLs), In: Proc. Transducers05, Seoul, (2005) 172-175.
- [10] Comi, C., Corigliano, A., Ghisi, A., Zerbini, S., A resonant micro accelerometer based on electrostatic stiffness variation, *Meccanica*, 48 (2013) 1893–1900.
- [11] Seshia, A.A., Howe, R.T., Montague, S., An integrated microelectromechanical resonant output gyroscope, In: Proc. MEMS2002, (2002) 722-726.
- [12] Li, J., Fang, J., Dong, H., Tao, Y., Structure design and fabrication of a novel dual-mass resonant output micromechanical gyroscope, *Microsyst. Technology*, 16, 4 (2010) 543- 552.
- [13] Comi, C., On geometrical effects in micro-resonators, *Latin American J. Solid and Structures*, 6 (2009) 73-87.
- [14] Ferrari, V., Ghisla, A., Marioli, D., Taroni, A., Silicon resonant accelerometer with electronic compensation of input-output cross-talk, *Sens. Actuator A, Phys.*, 123-124 (2005) 258-266.
- [15] Stoney, W., *Vibration of systems having distributed mass and elasticity*. Shock and Vibration Handbook, C. Harris, Ed. New York: McGrawHill, 1988.
- [16] Bokaian, A., Natural frequencies of beams under tensile axial load, *J.Sound Vib.*, 142 (1990) 481–498.
- [17] Tocchio, A., Comi, C., Langfelder, G., Corigliano, A., Longoni A., Enhancing the Linear Range of MEMS Resonators for Sensing Applications, *IEEE Sensors Journal*, 11(12) (2011) 3202-3210.
- [18] Caspani, A., Comi, C., Corigliano, A., Langfelder, G., Zega, V., Zerbini, S., Dynamic Non-Linear Behaviour of torsional resonators in MEMS, in preparation.